Transcriptomic profiling of sex-specific olfactory neurons reveals subset-specific receptor expression in *C. elegans*

Author Names and Affiliations:

Douglas K. Reilly[1,7,†], Erich M. Schwarz[2,†], Caroline S. Muirhead[1], Annalise N. Robidoux[1,3], Igor Antoshechkin[4], Anusha Narayan[4,5], Meenakshi K. Doma[4,6], Paul W. Sternberg[4], Jagan Srinivasan[1,8,*]

[1] Department of Biology and Biotechnology, Worcester Polytechnic Institute, Worcester, MA 01605, USA

[2] Department of Molecular Biology and Genetics, Cornell University, Ithaca, NY 14853, USA

[3] Department of Chemistry and Biochemistry, Worcester Polytechnic Institute, Worcester, MA 01605, USA

[4] Division of Biology and Biological Engineering, California Institute of Technology, Pasadena, CA 91125

[5] Present address: Strategic Marketing, Evidation Health, San Mateo, CA 94402, USA

[6] Present address: Genomics Lead, Individualized Cell and Gene Therapies, South San Francisco, Genentech, CA 94080, USA

[7] Present address: Biology Department, Tufts University, Medford, MA 02155, USA

[8] Program of Bioinformatics and Computational Biology, Worcester Polytechnic Institute, Worcester, MA 01605, USA

* Corresponding author

[†] These authors contributed equally to this work

22 **Short Title: Male pheromone G protein-coupled receptors in *C. elegans***

23

24 **Key words:** *C. elegans*, Pheromone, Sex-specific, G Protein-Coupled Receptors, Transcriptomes,

25 Single-Cell

26

27 **Corresponding author:**

28 Jagan Srinivasan

29 Life Sciences and Bioengineering Center, 4th Floor

30 60 Prescott Street, Worcester, MA, 01605

31 (508) 831-6564

32 jsrinivasan@wpi.edu

SUMMARY

The nematode *Caenorhabditis elegans* utilizes chemosensation to navigate an ever-changing environment for its survival. A class of secreted small-molecule pheromones, termed ascarosides, play an important role in olfactory perception by affecting a host of biological function ranging from development to behavior. The ascaroside ascr#8 mediates sex-specific behaviors, driving avoidance in hermaphrodites and attraction in males. Males sense ascr#8 via the ciliated male-specific cephalic sensory (CEM) neurons, which exhibit radial symmetry along dorsal-ventral and left-right axes. Calcium imaging studies suggest a complex neural coding mechanism that translates stochastic physiological responses in these neurons to reliable behavioral outputs. To test the hypothesis that the neurophysiological complexity arises from differential expression of genes within subsets of these neurons, we performed cell-specific transcriptomic profiling of these sensory neurons. Expression profiling revealed between 20 and 639 genes enriched at least two-fold per CEM neuron and identified multiple G protein coupled receptor (GPCR) candidates enriched in non-overlapping subsets of CEM neurons. GFP reporter analysis confirmed that RNA expression of two of the GPCR genes, *srw-97* and *dmsr-12*, is enriched in specific subsets of the CEM neurons. Single CRISPR-Cas9 knockouts of either *srw-97* or *dmsr-12* resulted in partial defects, while a double knockout of both *srw-97* and *dmsr-12* completely abolished the attractive response to ascr#8, suggesting that each receptor acts in a non-redundant manner in discrete olfactory neurons. Together, our results suggest that the evolutionarily distinct GPCRs SRW-97 and DMSR-12 act to facilitate male-specific sensation of ascr#8 through discrete subsets of CEM neurons.

54 **INTRODUCTION**

55 The ability of an organism to find a mate is critical to the survival of a species. Many species utilize
56 small molecule pheromones to signal mate location (PUNGALIYA *et al.* 2009; NARAYAN *et al.*
57 2016), sexual maturity (APRISON AND RUVINSKY 2015; APRISON AND RUVINSKY 2017), and
58 receptivity (HOUCK *et al.* 2007; JANG *et al.* 2017). These signals are sensed and processed through
59 the nervous system to generate proper behavioral and developmental responses. The nematode
60 *Caenorhabditis elegans* communicates with conspecifics almost exclusively using pheromones
61 called ascarosides (LUDEWIG *et al.* 2019; MCGRATH AND RUVINSKY 2019).

62 Ascarosides are a large, structurally conserved class of small molecule pheromones (VON
63 REUSS AND SCHROEDER 2015; ZHANG *et al.* 2017). Built in a modular fashion, they are composed
64 of a core ascarylose sugar and a fatty-acid derived side chain (BUTCHER *et al.* 2007; VON REUSS *et*
65 *al.* 2012; LUDEWIG *et al.* 2019). Ascarosides signal a host of environmental and developmental
66 information, including the sexual maturity and location of potential mates (NARAYAN *et al.* 2016;
67 APRISON AND RUVINSKY 2017). This communication system is conserved across nematodes, with
68 different species using different combinations of ascarosides or structural derivatives (CHOE *et al.*
69 2012; RAGSDALE *et al.* 2013; DONG *et al.* 2016; DONG *et al.* 2018; REILLY *et al.* 2019). While the
70 effects of some ascarosides are dependent on physiological state (BUTCHER *et al.* 2009; BUTCHER
71 2017; CHUTE *et al.* 2019), others are able to elicit sex-specific responses (PUNGALIYA *et al.* 2009;
72 NARAYAN *et al.* 2016; FAGAN *et al.* 2018).

73 Most neurons in the *C. elegans* nervous system are bilaterally symmetrical (WHITE *et al.*
74 1986), though radially symmetric classes of sensory neurons exist, such as the inner labial (IL1
75 and IL2) neurons (HRUS *et al.* 2007; WANG *et al.* 2014; WANG *et al.* 2015) which are required for
76 normal dauer development, nictation behavior, and foraging (LEE *et al.* 2012; SCHROEDER *et al.*

77 2013). *C. elegans* also has several sex-specific neurons, such as the HSN neuron (hermaphrodite-
78 specific neuron) involved in egg laying (APIRSON AND RUVINSKY 2019a; APIRSON AND RUVINSKY
79 2019b), and the MCM neurons in the male that contribute to neuronal plasticity and learning
80 (SAMMUT *et al.* 2015). However, while most male-specific neurons are located in the tail, the major
81 contributor to male-specific behaviors are the chemosensory CEM neurons, located in the amphid.
82 These four radially symmetric neurons have been found, through laser ablation,
83 electrophysiology, and calcium imaging studies to be involved in sensing the ascaroside
84 pheromones ascr#8 and ascr#3 (PUNGALIYA *et al.* 2009; NARAYAN *et al.* 2016; REILLY *et al.* 2017).
85 Ascr#3 plays a role in dauer formation, functioning alongside ascr#2 and ascr#4 as the "dauer
86 pheromone" (BUTCHER *et al.* 2008). Ascr#8, meanwhile, is unique in that it contains a *p*-
87 aminobenzoic acid moiety on its terminus (PUNGALIYA *et al.* 2009; ARTYUKHIN *et al.* 2018). We
88 have previously shown by both laser and genetic ablation experiments that ascr#8 is sensed
89 primarily by male-specific CEM neurons located in the head region of the male nervous system
90 (NARAYAN *et al.* 2016). In animals lacking CEM (through either genetic or laser ablation), the
91 response to ascr#8 is abolished, and further ablation of the ASK results in complete loss of the
92 ascr#3 response (NARAYAN *et al.* 2016). Through studies ablating three of the four CEM neurons,
93 leaving one CEM neuron intact, it was found that four CEM neurons cooperate to drive a tuned
94 response to an intermediate, 1 μM concentration of both ascr#3 and ascr#8 (NARAYAN *et al.* 2016).
95 Although CEM neurons are indeed the primary pathway by which male *C. elegans* sense
96 and response to ascr#8, this response is modulated by additional neural circuitry via neuropeptides.
97 The FMRFamide-like peptide gene *flp-3* encodes ten discrete peptides, some of which act through
98 two neuropeptide receptors both to repress *C. elegans*' normal avoidance of ascr#8, and to

99 simultaneously make *C. elegans* positively attracted to ascr#8 (REILLY *et al.* 2021). However, it
100 remains unknown how CEM neurons themselves sense and drive responses to ascr#8.

101 Calcium imaging and electrophysiological experiments demonstrated that CEM neurons
102 show variable responses to stimuli not only between different animals, but within a single animal
103 (NARAYAN *et al.* 2016; REILLY *et al.* 2017). While other neurons such as the stochastically
104 asymmetric AWC chemosensory neurons show variable calcium responses between different
105 animals, these responses are consistent between the left and right AWC neurons of a single animal
106 (COCHELLA *et al.* 2014). In contrast, we have observed that responses of individual CEM neurons
107 are stochastic within single animals, and yet four CEM neurons within one animal are somehow
108 consistently able to generate proper behavioral responses to both ascr#3 and ascr#8 (NARAYAN *et*
109 *al.* 2016). To understand this remarkable pattern of stochastic neuronal activity yielding consistent
110 neuronal outputs, it is imperative to uncover genes encoding components of the CEM response.

111 A recent study in *C. elegans* hermaphrodites generated transcriptomic landscapes of 118
112 neuronal classes from 302 neurons in order to link functional and anatomical properties of
113 individual neurons with their molecular identities (TAYLOR *et al.* 2021). Discrete neuronal classes
114 were successfully identified via their combinations of expressed neuropeptides and neuropeptide
115 receptor genes. However, a similar feat is yet to be performed on male *C. elegans*, and the
116 transcriptomic profiles of male neurons remain enigmatic.

117 In a more focused transcriptomic approach, gene expression profiles of extracellular
118 vesicle-releasing neurons (EVNs) as a whole were determined by expressing GFP under the EVN-
119 specific *klp-6* promoter, mechanically and proteolytically dissociating male worms expressing this
120 GFP, selecting the target GFP^+ neurons with FACS, and performing RNA-seq on the collected
121 GFP^+ neurons (WANG *et al.* 2015; KALETSKY *et al.* 2016). This gave thousands of EVNs in each

122 biological replicate and offered increased statistical power in analyzing transcriptional landscapes.
123 CEM neurons are a subset of EVN neurons, so CEM transcriptomic data are embedded in these
124 data, but the expression values of CEM and EVN are not equivalent.

125 To begin understanding how CEM neurons achieve stochastic yet reliable physiological
126 responses to ascr#8, we performed single-cell RNA-seq (SCHWARZ *et al.* 2012) on male-specific
127 CEM neurons. We uncovered a small number of genes encoding G protein-coupled receptors
128 (GPCRs) highly enriched in single CEM neurons. Given that all ascaroside receptors identified to
129 date have been GPCRs (KIM *et al.* 2009; MCGRATH *et al.* 2011; PARK *et al.* 2012; GREENE *et al.*
130 2016a; GREENE *et al.* 2016b; CHUTE *et al.* 2019), we tested whether any of these enriched genes
131 contribute to male *C. elegans* sensation of ascr#8. Through neuronal RNAi knockdown and
132 CRISPR null mutagenesis, we identified two distantly related GPCR genes that contribute to the
133 ascr#8 behavioral response, *srw-97* and *dmsr-12*; expression of these genes are enriched in ventral
134 and dorsal CEMs, respectively. When expression of each receptor was knocked down through
135 RNAi, behavioral responses to ascr#8 were partially deficient. Using CRISPR and genetic crosses
136 to generate a double *srw-97 dmsr-12* mutant, we found that loss of both receptors results in a
137 complete loss of behavioral response to ascr#8. Phylogenetic analysis further indicates that both
138 receptors are homologous to closely related receptors across the *Caenorhabditis* genus, and robust
139 ascr#8 responses may be a trait recently evolved in *C. elegans*.

140

141 **RESULTS**

142 **The transcriptomic landscape of CEM neurons is variable**

143 Individual CEM neurons were isolated from *C. elegans* expressing an integrated GFP
144 labeling extracellular vesicle-releasing neurons (EVNs, p*pkd-2*::GFP [**Figure 2A**]), as previously

145 described (GOODMAN *et al.* 1998; NARAYAN *et al.* 2011; NARAYAN *et al.* 2016). Cells were
146 separated by anatomical identity (i.e., CEM dorsal left [DL], dorsal right [DR], ventral left [VL],
147 and ventral right [VR]), and cDNA libraries were constructed.

148 Enriched genes in each CEM neuron were identified by comparing RNA-seq profiles of
149 distinct CEM types; genes expressed at least two times more strongly in one CEM type than others
150 were listed and checked for biological functions, as annotated by their WormBase Gene Ontology
151 (GO) terms (HARRIS *et al.* 2020; GENE ONTOLOGY 2021). A variety of enriched gene sets were
152 defined for different CEM neurons, ranging from 20 genes enriched in CEM VL to over 600 in
153 CEM VR (**Table S1, S6, S7**). Dorsal CEM neurons were more consistent, expressing 98 and 105
154 enriched genes in the right and left neurons, respectively (**Table S1, S8, S9**). Uniquely mapped
155 reads ranged from 1.9 to 3.8 million per CEM type, matching the trend for alignment rates of each
156 CEM neuron, which ranged from 19.73% to 48.01%, (**Table S2**) with an average of 1.410 genes
157 showing robust RNA expression in each neuron (**Table S3**).

158 Five genes encoding G protein-coupled receptors (*seb-3, srr-7, srw-97, dmsr-12, srd-32*)
159 were expressed at levels four times higher in one CEM neuron than in other CEM neurons. Of
160 these, four were uncharacterized; one (*seb-3*) has previously been shown to play roles in
161 locomotion, stress response, and ethanol tolerance (JEE *et al.* 2013). *dmsr-12* is related to *daf-37*
162 (ROBERTSON AND THOMAS 2006), a previously identified ascaroside receptor gene (PARK *et al.*
163 2012), although it is more closely related to the neuropeptide receptor gene *dmsr-1*, and more
164 distantly to *srw-97* (ROBERTSON AND THOMAS 2006). *srd-32* belongs to a divergent branch of the
165 SRD phylogeny, which is itself a divergent family of the STR superfamily (ROBERTSON AND
166 THOMAS 2006). *srr-7* belongs to the one of the smallest families of *C. elegans* chemoreceptor

genes, outside of the single opsin family member, *sro-1*, and the *srm* family encoding five chemoreceptor genes (ROBERTSON AND THOMAS 2006)).

seb-3 and *srw-97* exhibited similar enrichment profiles across the CEM neurons, with ~3.5-fold enrichment in CEM VR (**Table 1; Figure 1D; Table S7**). *dmsr-12* showed almost five-fold stronger expression in CEM DL versus other CEM neurons (**Table 1; Figure 1A; Table S8**), while *srd-32* was only 1.62-fold enriched (**Table 1; Figure 1A; Table S8**). *srr-7* showed only two-fold enrichment in CEM VL (**Table 1; Figure 1C; Table S6**), which correlated with previous transcriptomic analyses that found *srr-7* to be enriched in *C. elegans* EVNs (WANG *et al.* 2015).

CEM-specific receptor expression patterns

To confirm our single-cell RNA-seq results, we generated transgenic GFP fusions for the five receptor genes (BOULIN *et al.* 2006). Roughly 3 kb of promoter region upstream of the start codon was included in these constructs, along with the majority of the coding sequence (**Table S10**); this would have automatically included any large 5'-ward introns that might contain cis-regulatory elements of these genes (FUXMAN BASS *et al.* 2014). The GFP coding sequence was cloned from the Fire Kit vector pPD95.75 (BOULIN *et al.* 2006). *pha-1; lite-1; him-5* animals were injected with reporter constructs and the co-injection marker pBX (*pha-1*(+)).We isolated GFP^+ strains and imaged and GFP^+ males for expression at 63x magnification (**Figure 2; Fig. S1**). An integrated p*pkd-2*::GFP line was used as a CEM-specific control (**Figure 2A**).

The previously characterized GPCR gene, *seb-3*, displayed a non-CEM-specific expression pattern matching that previously described (**Figure 2B**) (JEE *et al.* 2013), and was excluded from further analyses. The other four receptor genes showed transgenic expression patterns similar to their RNA-seq data: GFP-tagged DMSR-12 was heavily enriched in CEM DL, but also exhibited

190 CEM DR expression, and was observed in both soma and cilia (**Figure 2C**). GFP-tagged SRD-32
191 was found faintly in both dorsal CEM neurons but exhibited no ciliary localization (**Figure 2D**).
192 GFP-tagged SRW-97 was found in both ventral CEM soma and cilia, with slightly higher
193 expression in CEM VL (**Figure 2E**). GFP-tagged SRR-7 was found in CEM VR, as well as another
194 neuron that is likely to be CEP VR (**Figure 2F**). As with *seb-3*, *srr-7* was excluded from further
195 analyses, as we aimed to identify CEM-specific regulators of the ascr#8 response.

196 Except for SRD-32, all GFP-tagged receptors showed subcellular localization patterns that
197 included the sensory cilia (**Figure 2, white bars**). Our failure to see this for SRD-32 may be an
198 artifact of our p*srd-32*::GFP construct design, because only 52% of the *srd-32* coding sequence
199 was included in our transgene (**Table S10**).

200 We also observed non-GPCR genes to be heavily enriched in single CEM neurons, such as
201 *trf-1*, which encodes a TNF receptor homolog (TENOR AND ABALLAY 2008); *trf-1* has an EVN-
202 specific promoter (WANG *et al.* 2015), which provides an alternative to the *pkd-2* and *klp-6*
203 promoters typically used to drive transgenes in EVNs (**Fig. S1**) (PEDEN AND BARR 2005; BAE *et*
204 *al.* 2006). This fits previous observations of *trf-1*::GFP expression in CEM, HOB, and RnB
205 neurons (WANG *et al.* 2015).

206

207 **RNAi-mediated knockdown of CEM Receptors**

208 To test whether these CEM-enriched genes encoded receptors that are required in ascr#8
209 sensation, we used RNAi in a strain that is hypersensitive to neuronal RNA interference,
210 *nre-1; lin-15B* (SCHMITZ *et al.* 2007; POOLE *et al.* 2011). We crossed *nre-1; lin-15B* from this
211 strain into a *him-5* background so that we could assay ascr#8 responses in males. Young adults
212 were then reared on NGM agar plates containing 1 mM IPTG to induce expression of dsRNA

213 within the food source which would cause receptor-specific RNAi. Young adult males of the
214 subsequent generation were then assayed for their response to ascr#8 after being grown on either
215 a control vector (pL4440) or targeted dsRNA vector.

216 To confirm that our system for male neuronal RNAi could affect behavioral phenotypes,
217 we first fed animals M02B7.3 (α-*osm-3*) and B0212.5 (α-*osm-9*) RNAi clones from the Ahringer
218 Library (FRASER *et al.* 2000; KAMATH *et al.* 2003). Using our single-worm Spot Retention Assay
219 (NARAYAN *et al.* 2016), we assayed animals subjected to RNAi against *osm-3* or *osm-9* for their
220 behavioral dwell time in ascr#8 (**Figure 3A**). Animals fed *osm-3* dsRNA showed significantly
221 defective responses to ascr#8, like that observed loss-of-function alleles (**Figure 3B**). In contrast,
222 animals fed *osm-9* showed only a slight decrease in their times spent within ascr#8 (**Figure 3A**).
223 Because we could successfully abolish ascr#8 attraction through male neuronal RNAi of *osm-3*,
224 we could be confident that RNAi would be broadly effective at functionally verifying CEM-
225 enriched genes encoding components of the ascr#8 response.

226 We thus fed animals dsRNA clones targeting three CEM-enriched receptor genes:
227 T18H12.5 (α-*srd-32*), H34P18.1 (α-*dmsr-12*), and ZC204.15 (α-*srw-97*). The α-*srd-32* clone was
228 the only one not available in the Ahringer library (FRASER *et al.* 2000; KAMATH *et al.* 2003), but
229 a clone from the Vidal library was available (RUAL *et al.* 2004). These clones were in the same
230 backbone vector, allowing for the same control vector to be utilized across studies.

231 RNAi of *srd-32* caused no defect in ascr#8 responses (**Figure 3C**). Either *dmsr-12* or *srw-*
232 97 dsRNA caused partial defects of ascr#8 dwell time (**Figure 3C**). Neither knockdown
233 statistically lowered the dwell time in ascr#8 (**Figure 3D**), though they did abolish the statistically
234 significant increase in time spent in ascr#8 over vehicle controls (**Figure 3C**).

235 **CRIPSR-generated null mutants of candidate receptors**

236 We used CRISPR to generate a null allele of *srw-97(knu456)* via InVivo Biosystems and
237 backcrossed it into a *him-5* background for analysis of male attraction to ascr#8. For phenotypic
238 analysis of null mutants, we used our Single Worm Attraction Assay (SWAA) (REILLY *et al.*
239 2021). In this assay, animals are placed in a well of a 48-well tissue culture plate containing NGM
240 coated in *E. coli* OP50, and either nothing (S), a drop of the vehicle control (V), or the attractive
241 ascaroside (A). The location of animals is recorded over 15 minutes, and the time spent in the
242 center of the well, or cue, is compared (REILLY *et al.* 2021).

243 Wild-type (*him-5*) animals were strongly attracted to ascr#8 in the SWAA, replicating our
244 previous observations (**Figure 4A, B; Fig. S2**) (REILLY *et al.* 2021). *srw-97(knu456)* males
245 displayed partially defective ascr#8 attraction: their ascr#8 dwell time was no different than that
246 of vehicle (**Figure 4B; Fig. S2**), while their increase over the vehicle was no different than that of
247 *him-5* (**Figure 4A; Fig. S2**).

248 We were able to restore normal ascr#8 attraction to *srw-97(knu456)* males through
249 transgenesis with a translational fusion construct (p*srw-97*::*srw-97*::GFP) that employed the same
250 promoter as our transcriptional fusion (**Figure 2E**). Expression of the rescue transgene matched
251 that of our initial fusion, with GFP visible in both ventral CEM neurons (**Figure 4C**). Single-worm
252 assays revealed that the *srw-97* rescue construct completely rescued the partial defect in the ascr#8
253 response (**Figure 4A, B; Fig. S2**).

254 We obtained a *dmsr-12(tm8706)* null allele from the National BioResource Program in
255 Japan and crossed it into a *him-5* background as well. Like *srw-97(knu456)*, *dmsr-12(tm8706)*
256 males exhibited partially defective responses to ascr#8 (**Figure 5A, B; Fig. S3**). Similarly, the
257 expression profile of the p*dmsr-12*::*dmsr-12*::GFP rescue construct matched its earlier reporter

258 expression (**Figure 2C, 5C**). This rescue construct also completely restored normal attraction to
259 ascr#8 (**Figure 5A, B; Fig. S3**).

260 Given that *dmsr-12* is expressed in dorsal CEM neurons, and *srw-97* is expressed in ventral
261 CEM neurons (**Figure 2C, E**), we speculated that single mutants of either *dmsr-12* or *srw-97*
262 partially retained the ability to sense and respond to ascr#8, with the opposing wild-type CEM-
263 specific receptor gene conferring some residual response to ascr#8. We thus generated a *dmsr-*
264 *12; srw-97* double mutant strain and assayed animals for their ability to respond to ascr#8. These
265 double mutants completely failed to be attracted to or retained by ascr#8 activity (**Figure 5; Fig.**
266 **S3**). This defect, though strong, was specific to ascr#8 sensation; double mutants showed no defect
267 in their responses to ascr#3 (**Figure 5D, E; Fig. S4**).

268 Together, these data suggest that at least two GPCR receptors are expressed in opposite
269 pairs of CEM neurons and act in parallel during sensation of ascr#8.

270

271 **Phylogenetic analyses of ascr#8 receptors reveal likely gene duplication events**

272 The ability to attract mates through pheromones is often essential for a species' survival.
273 However, *C. elegans* is a self-fertile hermaphrodite: male mating is useful in creating genetic
274 diversity but is not absolutely required for species propagation. We have recently observed that
275 different *Caenorhabditis* species show quite different responses to ascr#8 (REILLY *et al.* 2019).
276 To understand this pattern better, we analyzed the evolution of both *srw-97* and *dmsr-12*.

277 We identified orthologs of *srw-97* from *C. elegans* (*Cel-srw-97*) in other *Caenorhabditis*
278 proteoms via OrthoFinder (**Figure 6A**). A closely related *C. elegans* paralog, *Cel-srw-98*,
279 underwent a species-specific expansion within *C. inopinata*. However, other species, such as
280 *C. briggsae* and *C. nigoni*, have closely related paralogs to *Cel-srw-97*. The coding DNA

281 sequences (CDS DNAs) of both *Cel-srw-97* and *Cel-srw-98* are 66.2% identical to one another,
282 while their amino acid sequences are only 57.1% identical (MADEIRA *et al.* 2019). In our single-
283 cell CEM RNA-seq data, *Cel-srw-98* shows enrichment similar to that of to *Cel-srw-97*; it is most
284 strongly expressed in CEM VR, although below the two-fold enrichment cutoff that we chose in
285 selecting candidates for functional analysis (**Table 1**).

286 *C. tropicalis*, like *C. elegans* and *C. briggsae*, is a hermaphroditic *Caenorhabditis* species
287 for which male mating is optional (NOBLE *et al.* 2021). *C. tropicalis* encodes a reduced number of
288 ascr#8 receptor gene paralogs, with no *Cel-dmsr-12* paralogs, and only one *Cel-srw-97* paralog
289 (**Figure 6**). We previously observed that *C. tropicalis* fails to be attracted to ascr#8, and it is
290 possible that this loss of receptor genes is one reason for that failure (REILLY *et al.* 2019). Given
291 the conserved activity of cis-regulatory elements between different *Caenorhabditis* species (WANG
292 *et al.* 2004; GORDON *et al.* 2015), it would be interesting to express a *Cel-srw-97* construct in *C.*
293 *tropicalis* to see if it can confer attraction to and retention by ascr#8.

294 In contrast, the other candidate ascr#8 receptor, *dmsr-12*, does not appear in our
295 phylogenetic analysis to have undergone any species-specific expansion (**Figure 6B**). In fact,
296 outside of *C. elegans*, there are generally fewer paralogs per species. The most closely related *C.*
297 *elegans* gene in our phylogeny, *Cel-dmsr-13*, does not show CEM enrichment in our single-neuron
298 RNA-seq data, although *Cel-dmsr-10*, *Cel-dmsr-11*, and *Cel-dmsr-16* are somewhat enriched
299 within CEM VR (**Table S7**). Notably, CEM VR is the same neuron in which *srw-97* is enriched.
300

301 **DISCUSSION**

302 Pheromones are important for mating in many animals. In the nematode *C. elegans*, males are
303 attracted to hermaphrodites as possible mates by the small molecule pheromone ascaroside #8

304 (PUNGALIYA *et al.* 2009; NARAYAN *et al.* 2016). While the ascaroside class of small molecule
305 pheromones utilized by nematodes is rapidly being elucidated (with over 230 known ascaroside
306 structures so far; *https://smid-db.org*) (ARTYUKHIN *et al.* 2018), the neuronal receptor proteins that
307 mediate pheromone signals remain largely unknown. For only a select few ascarosides have
308 sensory components been identified at the cellular (GREENE *et al.* 2016a; GREENE *et al.* 2016b;
309 CHUTE *et al.* 2019), receptor (KIM *et al.* 2009; MCGRATH *et al.* 2011; PARK *et al.* 2012), or signal
310 transduction levels (ZWAAL *et al.* 1997).

311 Here, we identify two novel G protein-coupled receptors as active, required components in
312 the sensation and behavioral response to the mating pheromone, ascr#8. Transcripts for the two
313 GPCRs, *dmsr-12* and *srw-97*, are enriched in single CEM neurons (**Table 1**), and they express in
314 non-overlapping subsets of the male-specific chemosensory neurons (**Figure 1, 2**). There are,
315 however, other receptors present in these same neurons that contribute to the navigation of a vast
316 and ever-changing array of environmental cues, such as the widely expressed ethanol sensor, *seb-*
317 *3* (**Figure 2B**) (JEE *et al.* 2013).

318 One mechanism for sensory flexibility in CEM neurons may be heterodimerization of
319 receptor proteins. Previous work identified two receptors for ascr#2 in the ASK neuron: DAF-37
320 and DAF-38 (PARK *et al.* 2012). While both are required for proper ascr#2-induced dauer
321 formation, only DAF-38 is involved in the sensation of other ascarosides (PARK *et al.* 2012). Such
322 heterodimers may also exist for pheromone receptors in CEM neurons.

323 Another mechanism for sensory flexibility in CEM neurons is to have diverse receptor
324 proteins with distinct specificities co-expressed within a single neuron. Multiple ascarosides are
325 sensed by the male-specific CEM neurons, including ascr#8 and ascr#3 (NARAYAN *et al.* 2016).
326 The two receptors identified here may function as ascr#8-specific receptors, as *dmsr-12;srw-97*

327 double mutant animals do not exhibit defective responses to ascr#3 (**Figure 5D, E**). The related
328 receptors *dmsr-10*, *dmsr-13*, *dmsr-16*, and *srw-98* are enriched in ventral CEM neurons, and may
329 heterodimerize with *srw-97*, to result in fine-tuned sensation of ascr#8. Similarly, there may be
330 other receptors may be enriched in the dorsal CEM neurons to heterodimerize with *dmsr-12*. The
331 role of DAF-37 as an ascr#2-specific receptor further supports our hypothesis, as *dmsr-12* is related
332 to DAF-37 (ROBERTSON AND THOMAS 2006). The ventral CEM-receptor, *srw-97* falls within the
333 same large family of GPCRs as well (KRISHNAN *et al.* 2014), while the promiscuous DAF-38 does
334 not (ROBERTSON AND THOMAS 2006).

335 The initial goal of our single-cell RNA-seq analysis of male-specific chemosensory CEM
336 neurons was to identify GPCRs encoding pheromone receptors. However, further analysis of other
337 genes with CEM-enriched expression should also uncover specific and novel promoter profiles,
338 which will enable optogenetic manipulation and calcium imaging of defined individual CEM
339 neurons (NARAYAN *et al.* 2016). The development of advanced transgenic reagents will also permit
340 chemical biology of CEM neurons. We have recently developed an active ascr#8 bioaffinity probe
341 to employ in the targeted elucidation of ascr#8 receptors (ZHANG *et al.* 2019). Use of this probe
342 will lead to further elucidation of the identity of acsr#8 receptors, by confirming either SRW-97
343 or DMSR-12 as receptors or identifying their heterodimeric partners. The combination of these
344 technologies should clarify how heterogeneous CEM neurons achieve homogeneous sensory
345 responses.

346 **METHODS**

347 **Single cell isolation and RT-PCR**

348 Microdissection and single-cell RT-PCR of individual CEM_DL, CEM_DR, CEM_VL,
349 and CEM_DR neurons was performed essentially as described (SCHWARZ *et al.* 2012). For all four
350 neuronal types, single-end 50-nucleotide (nt) RNA-seq was performed on an Illumina HiSeq 2000.
351 To identify so-called housekeeping genes and genes primarily active outside the nervous system,
352 we compared our results from CEM_DL, CEM_DR, CEM_VL, and CEM_DR to equivalent
353 analyses of published single-end 38-nt RNA-seq data from mixed-stage whole *C. elegans*
354 hermaphrodite larvae (SCHWARZ *et al.* 2012).

355

356 **Transcriptional analysis**

357 Reads were quality-filtered as follows: neuronal reads that failed Chastity filtering were
358 discarded (Chastity filtering had not been available for the larval reads); raw 38-nt larval reads
359 were trimmed 1 nt to 37 nt; all reads were trimmed to remove any indeterminate ("N") residues or
360 residues with a quality score of less than 3; and larval reads that had been trimmed below 37 nt
361 were deleted, as were neuronal reads that had been trimmed below 50 nt. This left a total ranging
362 from 21,554,964 (CEM_VL) to 24,546,096 (CEM_DL) filtered reads for analysis of each neuronal
363 type, versus 23,369,056 filtered reads for whole larvae (**Table S2**).

364 We used RSEM version 1.2.17 (LI AND DEWEY 2011) with bowtie2 version 2.2.3
365 (LANGMEAD AND SALZBERG 2012) and SAMTools version 1.0 (LI *et al.* 2009) to map filtered reads
366 to a *C. elegans* gene index and generate read counts and gene expression levels in transcripts per
367 million (TPM). To create the *C. elegans* gene index, we ran RSEM's *rsem-prepare-reference* with
368 the arguments '*--bowtie2 --transcript-to-gene-map*' upon a collection of coding DNA sequences

369 (CDSes) from both protein-coding and non-protein-coding *C. elegans* genes in WormBase release
370 WS245 (HOWE *et al.* 2016). The CDS sequences were obtained from *ftp://ftp.sanger.ac.uk/pub2/*
371 *wormbase/releases/WS245/species/c_elegans/PRJNA13758/c_elegans.*
372 *PRJNA13758.WS245.mRNA_transcripts.fa.gz* and *ftp://ftp.sanger.ac.uk/pub2/wormbase/*
373 *releases/WS245/species/c_elegans/PRJNA13758/c_elegans.PRJNA13758.WS245.ncRNA_*
374 *transcripts.fa.gz*. For each RNA-seq data set of interest, we computed mapped reads and
375 expression levels per gene by running RSEM's *rsem-calculate-expression* with the arguments
376 '*--bowtie2 -p 8 --no-bam-output --calc-pme --calc-ci --ci-credibility-level*
377 *0.99 --fragment-length-mean 200 --fragment-length-sd 20 --estimate-rspd --ci-memory 30000*'.
378 These arguments, in particular '*--estimate-rspd*', were aimed at dealing with single-end data from
379 3'-biased RT-PCR reactions; the arguments '*--phred33-quals*' and '*--phred64-quals*' were also used
380 for the neuronal and larval reads, respectively. We computed posterior mean estimates (PMEs)
381 both for read counts and for gene expression levels, and rounded PMEs of read counts down to the
382 nearest lesser integer. We also computed 99% credibility intervals (CIs) for expression data, so
383 that we could use the minimum value in the 99% CI for TPM as a robust minimum estimate of a
384 gene's expression (minTPM).

385 We observed the following overall alignment rates of the reads to the WS245 *C. elegans*
386 gene index: 48.01% for the CEM_DL read set, 28.19% for the CEM_DR read set, 40.75% for the
387 CEM_VL read set, 19.73% for the CEM_VR read set, and 76.41% for the larval read set (**Table**
388 **S2**). A similar discrepancy between lower alignment rates for hand-dissected linker cell RNA-seq
389 reads versus higher alignment rates for whole larval RNA-seq reads was previously observed, and
390 found to be due to a much higher rate of human contaminant RNA sequences in the hand-dissected
391 linker cells (SCHWARZ *et al.* 2012). We defined detectable expression for a gene in a given

392 RNA-seq data set by that gene having an expression level of 0.1 TPM; we defined robust
393 expression by that gene having a minimum estimated expression level (termed minTPM) of at least
394 0.1 TPM in a credibility interval of 99% (i.e., ≥ 0.1 minTPM). The numbers of genes being scored
395 as expressed in a given neuronal type above background levels, for various data sets, are given in
396 **Table S3**. Other results from RSEM analysis are given in **Table S3**.

397 We annotated *C. elegans* genes and the encoded gene products in several ways (**Table S5**).
398 For the products of protein-coding genes, we predicted classical signal and transmembrane
399 sequences with Phobius 1.01 (KÄLL *et al.* 2004), regions of low sequence complexity with pseg
400 (SEG for proteins, from *ftp://ftp.ncbi.nlm.nih.gov/pub/seg/pseg*) (WOOTTON 1994), and coiled-coil
401 domains with ncoils (from *http://www.russell.embl-heidelberg.de/coils/coils.tar.gz*) (LUPAS
402 1996). PFAM 27.0 protein domains from PFAM (FINN *et al.* 2016) were detected with HMMER
403 3.0/hmmsearch (EDDY 2009) at a threshold of $E \leq 10^{-5}$. The memberships of genes in orthology
404 groups from eggNOG 3.0 (POWELL *et al.* 2012) were extracted from WormBase WS245 with the
405 TableMaker function of ACEDB 4.3.39. Genes with likely housekeeping status (based on
406 ubiquitous expression in both larvae and linker cells) were as identified in our previous work
407 (SCHWARZ *et al.* 2012). Genes were predicted to encode GPCRs on the basis of their encoding a
408 product containing one or more of the following Pfam-A protein domains: 7tm_1 [PF00001.16],
409 7tm_2 [PF00002.19], 7tm_3 [PF00003.17], 7tm_7 [PF08395.7], 7TM_GPCR_Srab [PF10292.4],
410 7TM_GPCR_Sra [PF02117.11], 7TM_GPCR_Srbc [PF10316.4], 7TM_GPCR_Srb
411 [PF02175.11], 7TM_GPCR_Srd [PF10317.4], 7TM_GPCR_Srh [PF10318.4], 7TM_GPCR_Sri
412 [PF10327.4], 7TM_GPCR_Srj [PF10319.4], 7TM_GPCR_Srsx [PF10320.4], 7TM_GPCR_Srt
413 [PF10321.4], 7TM_GPCR_Sru [PF10322.4], 7TM_GPCR_Srv [PF10323.4], 7TM_GPCR_Srw
414 [PF10324.4], 7TM_GPCR_Srx [PF10328.4], 7TM_GPCR_Srz [PF10325.4], 7TM_GPCR_Str

415 [PF10326.4], ABA_GPCR [PF12430.3], Sre [PF03125.13], and Srg [PF02118.16]. By this
416 criterion, we identified 1,615 genes encoding GPCRs in the WS245 version of the *C. elegans*
417 genome; this resembles a previous estimate of ~1,470 *C. elegans* genes encoding chemoreceptors
418 and other GPCRs, identified through extensive computational and manual analysis (HOBERT
419 2013). The memberships of genes in orthology groups from eggNOG 3.0 (POWELL *et al.* 2012)
420 were extracted directly from WormBase WS245 with the TableMaker function of ACEDB 4.3.39.
421 Genes with likely housekeeping status (based on ubiquitous expression in both larvae and linker
422 cells) were as identified in our previous work (SCHWARZ *et al.* 2012). Gene Ontology (GO)
423 annotations for *C. elegans* genes were extracted from WormBase-computed annotations in *ftp://*
424 *ftp.wormbase.org/pub/wormbase/releases/WS245/ONTOLOGY/*
425 *gene_association.WS245.wb.c_elegans*; human-readable text descriptions for GO term IDs were
426 extracted from *term.txt* in the Gene Ontology archive *http://archive.geneontology.org/full/2014-*
427 *07-01/go_201407-termdb-tables.tar.gz*.
428

429 **GFP reporter construction**

430 Reporter fusion constructs were generated using previously described techniques (BOULIN
431 *et al.* 2006). Approximately 2-3 kb of upstream promoter region of each gene was included in
432 construct generation, as well as a portion of the coding sequence (**Table S10**). This was then fused
433 to GFP (from the Fire Vector Kit plasmid, pPD95.75), via PCR fusion (BOULIN *et al.* 2006).
434 Primers were designed using Primer 3 and ordered from IDT (Integrated DNA Technologies).
435 Primer sequences available in **Table S12**. Successful fusion was confirmed via gel electrophoresis
436 prior to injection.

437 Reporter fusion constructs were injected into the gonads of *pha-1(e2123ts); lite-1(ce314);*
438 *him-5(e1490)* animals, along with a co-injection marker of pBX(*pha-1*(+)). In this manner, positive
439 array animals will propagate normally at 20 °C. Strains were confirmed via GFP expression, with
440 multiple array lines being generated per injection (**Table S11**). Injections were performed by
441 InVivo Biosystems, with strain isolation being performed in house.
442
443 **Imaging**
444 Animals were imaged for GFP expression using previously described techniques. GFP+
445 young adult male animals were mounted on a 1% agarose pad and immobilized with sodium azide.
446 Animals were then imaged on a spinning disk confocal microscope at 63x magnification. Z-stack
447 imaging was performed, generating 3D reconstructions of the heads of the imaged animals.
448 Central/optimal z-plane images were used to generate the images used to verify expression (**Figure**
449 **2; Fig. S1**).
450
451 **RNAi Feeding**
452 VH624 (*rhIs13* [*unc-119*::GFP + *dpy-20*(+)]; *nre-1(hd20)*; *lin-15B(hd126)*) animals
453 (SCHMITZ *et al.* 2007; POOLE *et al.* 2011) were crossed with *him-5(e1490)* animals to integrate
454 male production into a strain hypersensitive to neuronal RNAi-knockdown, generating JSR44
455 (*nre-1(hd20)*; *lin-15B(hd126); him-5(e1490)*). During the cross, insertion of the *him-5(e1490)*
456 allele displaced the integrated array *rhIs13*, suggesting location of the array on Chromosome V.
457 Presence of *lin-15B(hd126)* in JSR44 was confirmed via sequencing. The non-annotated
458 *nre-1(hd20)* is linked with *lin-15B*, being retained alongside *lin-15B* (SCHMITZ *et al.* 2007; POOLE
459 *et al.* 2011).

460 RNAi clones were grown overnight in cultures of LB containing 50 µg/mL ampicillin.
461 Cultures were then diluted to an OD_{600} of 1.0 before plating on NGM agar plates containing 50
462 µg/mL ampicillin and 1 mM IPTG (Isopropyl-β-D-thiogalactoside) to select for RNAi clones and
463 induce expression. Lawns were allowed to grow at room temperature for 8-16 hours, before JSR44
464 young adult hermaphrodites were placed on the plates and left to propagate at 16°C. Young adult
465 males of the F1 progeny were then selected for behavioral testing suing the *Spot Retention Assay*.
466 Empty vector controls (VC-1 clone) were run alongside every targeted knockdown experiment.
467

468 **Spot Retention Assay**

469 Following previously described methods, young adult males were isolated from
470 hermaphrodites 5-16 hours prior to testing (PUNGALIYA *et al.* 2009; NARAYAN *et al.* 2016). In
471 short, at the time of the assay, 0.6 µL of either vehicle control (-) or ascaroside #8 (+) was added
472 to the NGM plates covered in a thin lawn of OP50 *E. coli*. Ten males were then divided between
473 two pre-marked spots on the agar, equidistant from the cues. The plate was then recorded for 20
474 minutes. The time spent of each visit in either vehicle or ascaroside #8 (if greater than 10 seconds)
475 was scored, and averaged. Plates in which the average was greater than two standard deviations
476 removed from the population average were removed from the final analysis as outliers. To
477 compare between strains or conditions, the vehicle was subtracted from the ascaroside dwell time
478 for each plate. The average of these differences was then compared statistically.
479

480 **Single Worm Behavioral Assay**

481 Following previously described methods (PUNGALIYA *et al.* 2009; NARAYAN *et al.* 2016;
482 REILLY *et al.* 2021), animals were isolated and prepared in an identical manner to the Spot

483 Retention Assay. The two outside rings of wells in a 48-well tissue culture plate were filled with
484 200 µL of NGM agar, which was then seeded with 65 µL of OP50 *E. coli*. The plates and lawns
485 were then dried at 37 °C for 4 hours. Alternating wells were then prepared as spatial controls
486 (nothing done), vehicle controls (0.85 µL of dH_2O was placed in the center of the well), or
487 ascaroside well (0.85 µL of ascaroside was placed in the center of the well). This was performed
488 over four quadrants. Animals were scored for their visits and duration to the center of the well
489 and/or the cue.

490 The average duration of each worm's visits was calculated, and these values were again
491 averaged together to generate a Mean Dwell Time in seconds for each plate. When comparing
492 across strains or conditions, the Spatial controls were then compared for statistical difference. If
493 none was observed, the Log(fold-change) A/V was then calculated by taking the log of the
494 ascaroside mean dwell time divided by the vehicle mean dwell time for each plate. The amount of
495 times each worm visited the center was averaged to generate the Visit Counts.

496 The Percent Attraction values were calculated by first determining the "attractive" cut off
497 as two standard deviations above the vehicle average. Any visit longer than this was deemed
498 "attractive" and scored as a "1"; non-attractive visits were scored as "0". The percent attraction
499 was then calculated for each worm was the percent of visits scored a "1". The average was then
500 calculated across the plate to determine Percent Attraction.

501

502 **CRISPR Design and Strain Generation**

503 A novel null mutation was generated for *srw-97* by InVivo Biosystems. The *srw-*
504 *97(knu456)* allele was generated in a *him-5(e1490)* strain using two sgRNAs
505 (TTTAGTAGAGCAGAAATTAA and TACAGCTTTAACTTTCAAC) to generate a 1,620-nt

506 deletion which removed the start codon and left only the terminal exon intact. The *knu456*
507 knockout allele was generated by donor homology using the pNU1361odn oligo:
508 (TTTTCTTGTATTTCCAAAAATTGTAAAAACCTTTATGAAAGTTAAAGCTGTAAGGAT
509 TTTCAGACATTTA). Following generation of a homozygous deletion by InVivo Biosystems,
510 the line was then backcrossed twice into *him-5(e1490)*.

511 The *dmsr-12(tm8706)* allele, provided by the National BioResource Group (NRBP)
512 contains a 118-nucleotide deletion that was generated by Dr. Mitani of the NRBP. The allele was
513 crossed into a *him-5(e1490)* background prior to testing. The deletion spans intron 2 and exon 3
514 of the coding sequence. Whether this results in a correctly spliced gene remains unknown, although
515 the expected remaining coding sequence remains in frame.

516

517 **Phylogenetic Analyses**

518 For phylogenetic analysis of selected CEM genes, we downloaded proteomes for
519 *C. elegans* and related *Caenorhabditis* nematodes from WormBase (release WS275), the Blaxter
520 *Caenorhabditis* database (release 1), or our unpublished work, as listed in **Table S4**. From each
521 proteome, we extracted the longest predicted isoform for each gene with *get_largest_isoforms.pl*
522 (*https://github.com/SchwarzEM/ems_perl/blob/master/fasta/get_largest_isoforms.pl*). We
523 observed that the predicted isoform for *dmsr-12* in the WormBase WS275 release of *C. elegans*'
524 proteome was shorter than past versions of *dmsr-12*, and that the WS275 isoform omitted exons
525 that our transgenic expression data (based on older gene models for *dmsr-12*) indicated were likely
526 to be real. We therefore manually replaced the WS275 version of *dmsr-12* with an older version
527 (extracted from the *C. elegans* proteome in the WS250 release of WormBase). We then computed
528 orthology groups for *C. elegans* and its related species with OrthoFinder version 2.3.11 (EMMS

529 AND KELLY 2015; EMMS AND KELLY 2019), using the arguments '*-a 1 -S diamond -og*'. We
530 identified which orthology groups contained the *C. elegans* genes *srr-7*, *srw-97*, and *dmsr-12*, and
531 extracted their sequences from a concatenation of all 11 proteomes via *extract_fasta_subset.pl*
532 (*https://github.com/SchwarzEM/ems_perl/blob/master/fasta/extract_fasta_subset.pl*). For each
533 orthogroup's member sequences, we aligned the sequences with MAFFT version 7.455 (KATOH
534 AND STANDLEY 2013) and filtered the alignments twice with trimAl version 1.4.rev15 (CAPELLA-
535 GUTIÉRREZ *et al.* 2009), using first the argument '*-automated1*' and then the arguments '*-resoverlap*
536 *0.50 -seqoverlap 50*'. From the filtered alignments, we computed maximum-likelihood protein
537 phylogenies with IQ-TREE version 2.0-rc1 (NGUYEN *et al.* 2015; KALYAANAMOORTHY *et al.*
538 2017), using the arguments '*-m MFP -b 100 --tbe*'. In particular, we used transfer bootstrap
539 expectation ('*--tbe*') which provides more reliable confidence values than classic bootstrapping
540 (LEMOINE *et al.* 2018). We visualized the resulting phylogenies with FigTree version 1.4.4 (*http:/*
541 */tree.bio.ed.ac.uk/software/figtree*).
542
543 **Statistical Analyses**
544 Prior to any statistical analyses, outliers were identified and removed. Outliers were
545 defined as any data points greater than two standard deviations removed from the average. All data
546 were then tested for normality using a Shapiro-Wilk Normality Test. This test was chosen over the
547 more conventional D'Agostino-Pearson Normality Test as many data sets were below 10 in
548 number (due to the statistical power offered by the Single Worm Behavioral Assay (REILLY *et al.*
549 2021).
550 The Spot Retention Assay data was analyzed using paired *t*-tests or Wilcoxon Matched-
551 Pairs Signed Rank tests to compare vehicle control and ascaroside dwell times within strains

552 following tests for normality (**Figure 3**). When comparing the values of multiple conditions or
553 strains, the data was first normalized to account for vehicle dwell time variation between plates
554 using a base-2 exponentiation, as described previously, to transform all data points into non-zero
555 values. This allows for the calculation of the fold-change as the log(base2) of the ascaroside dwell
556 time divided by the vehicle dwell time. These normalized values were then compared using a
557 Mann-Whitney test or a One-Way ANOVA followed by a Dunnett's multiple comparisons test
558 (**Figure 3**).

559 The Single Worm Behavioral Assay was first analyzed within each strain by performing
560 either a Repeated-Measures ANOVA followed by a Dunnett's multiple comparisons test or
561 Friedman test followed by Dunn's correction, comparing both Spatial control and Ascaroside
562 dwell times to that of the Vehicle Control. The log(fold-change) of raw ascaroside and vehicle
563 dwell time values were calculated and compared using either a One-Way ANOVA followed by a
564 Bonferroni's multiple corrections test or Friedman Test followed by Dunn's correction (**Figure 4,**
565 **5**). The ascr#3 log(fold-change) values were compared using a Student's *t*-test (**Figure 5E**). Visit
566 Counts were compared in the same manner as the Mean Dwell Time data, while the Percent
567 Attraction data was analyzed using paired *t*-tests or Wilcoxon Matched-Pairs Signed Rank tests to
568 compare the attractive values of the vehicle and ascaroside (**Figures S2, S3, S4**).

569

570 **Data availability**

571 RNA-seq reads will be submitted to the Sequence Read Archive (SRA; *https://*
572 *www.ncbi.nlm.nih.gov/sra*).

573

574 **ACKNOWLEDGEMENTS**

575 We thank the *Caenorhabditis* Genetics Center, which is funded by the NIH Office of
576 Research Infrastructure Programs (P40 OD01044), as well as the National BioResource
577 Project, L. Rene Garcia (Texas A&M University), and Douglas Portman (University of
578 Rochester Medical Center) for providing strains. We also thank InVivo Biosystems for
579 generating transgenic and CRISPR knockout animals. The synthetic ascr#8 utilized in this
580 study was provided by Frank Schroeder (Cornell University). The research reported in this
581 publication was supported by NIH R01 DC016058 (J.S.), R01 GM084389 (P.W.S.), the Howard
582 Hughes Medical Institute (P.W.S.), Moore Foundation Grant No. 4551 (E.M.S.), and Cornell
583 startup funding (E.M.S.). We thank Titus Brown and the Michigan State University High-
584 Performance Computing Center (supported by U.S. Department of Agriculture grant 2010-65205-
585 20361 and NIFA–National Science Foundation (NSF) grant IOS-0923812) for computational
586 support; additional computing was enabled by start-up and research allocations from NSF XSEDE
587 (TG-MCB180039 and TG-MCB190010).

588 **FIGURE AND TABLE LEGENDS**

Gene	CEM DL	CEM DR	CEM VL	CEM VR	Max CEM
pkd-2	1.30	0.09	0.25	0.77	143
seb-3	0.15	0.31	0.23	**3.25**	6.50
dmsr-12	**4.96**	0.06	0.04	0.11	4.96
srd-32	**1.62**	0.38	0.23	0.62	4.33
srw-97	0.14	0.27	0.18	**3.67**	5.50
srr-7	0.16	0.26	**1.90**	0.53	6.33
trf-1	0.00	0.00	0.00	226.28	226.28

589 **Table 1. Enrichment levels of candidate GPCR genes in CEM neurons.** Enrichment levels
590 displayed as normalized count within a single CEM cell type over the normalized count in the
591 remaining three CEM neurons. Max CEM is the enrichment in all four CEM neurons over the
592 remainder of the animal. The CEM with highest enrichment of each GPCR gene are denoted by
593 bolded-underlined values.

594

595 **Figure 1. Transcriptomic landscapes of the CEM neurons. (A-D)** TPKM plots of individual
596 CEM DL **(A)**, CEM DR **(B)**, CEM VL **(C)**, and CEM VR **(D)** neurons. X-axes display enrichment
597 in individual CEM neurons compared to whole larvae, while the Y-axes display total transcript
598 counts (TPM). Genes of interest are denoted by colored symbols, defined in the legend.

599

600 **Figure 2. Expression profiles of CEM-enriched GPCR genes of interest.** Transcriptional GFP
601 fusions of GPCR genes enriched in the CEM neurons. **(A)** A previously published CEM reporter,
602 p*pkd-2*::GFP. **(B)** p*seb*-3::GFP, matching previously published expression, with no discernable
603 enrichment in the CEM. **(C)** p*dmsr-12*::GFP is strongly expressed in the CEM DL neuron, as well
604 as the CEM DR soma. **(D)** p*srd-32*::GFP is weakly expressed in the somas of CEM DR and DL.
605 **(E)** p*srw-97*::GFP is expressed in both CEM VR and VL, with localization in the cilia as well as

606 the soma. **(F)** p*srr-7*::GFP is expressed in CEM VR, both the soma and cilia, as well the cilial of
607 a neighboring neuron, presumably CEP VR. Dorsal/ventral axes and anterior/posterior directions
608 shown in (B). Scale bars denote distal, cilia region.
609
610 **Figure 3. Knockdown of CEM-enriched GPCR candidates results in aberrant behavioral**
611 **response to ascr#8. (A)** Raw dwell times and **(B)** Log2(fold-change of ascr#8/vehicle) of RNAi
612 knockdown of the kinesin motor, *osm-3*, and the TRPV channel, *osm-9* confirm the ability of RNAi
613 feeding to affect pheromone-driven behaviors in a targeted manner. $n \geq 5$. **(C)** Raw dwell times
614 and **(D)** Log2(fold-change) of genetic null *osm-3* mutants reveal an inability to respond to ascr#8.
615 $n \geq 17$. **(E)** Raw dwell time and **(F)** Log2(fold-change) of GPCR of interest (*srd-32*, *dmsr*-12, and
616 *srw-97*) knockdown reveals *dmsr-12* and *srw-97* as contributors to the ascr#8 behavioral response.
617 $n \geq 4$. Error bars denote SEM. **(A, C, E)** Paired *t*-tests and Wilcoxon tests of vehicle control versus
618 ascr#8 dwell time, **(B)** ANOVA, followed by Bonferroni post-hoc tests comparing Log2(fold-
619 change) of RNAi knockdowns to VC-1 control and to each other, **(D)** Mann-Whitney test
620 comparing *him-5* and *osm-3* Log2(fold-change) in response to ascr#8, **(F)** ANOVA, followed by
621 Dunnett's post-hoc test comparing Log2(fold-change) of RNAi knockdowns to VC-1 control. * p
622 < 0.05, ** $p < 0.01$, **** $p < 0.0001$.
623
624 **Figure 4. The GPCR, SRW-97, is involved in the ascr#8 behavioral response. (A)** Raw dwell
625 times and **(B)** Log(fold-change) of *srw-97* knockout and transgenic rescue (WorEx57) animals.
626 **(C)** Expression of WorEx57 (p*srw-97*::*srw-97*::GFP) in CEM VR. Anterior/Posterior and
627 Right/Left axes denoted. Error bars denote SEM. $n \geq 5$. **(A)** ANOVA followed by Dunnett's post-

628 hoc test or Friedman test followed by Dunn's (within strain), **(B)** Friedman test, followed by
629 Dunn's post-hoc test (between strain log(fold-change) values). * $p < 0.05$, ** $p < 0.01$.
630
631 **Figure 5. The DMSR-12 receptor acts in non-SRW-97-expressing CEM neurons to aid in**
632 **driving the ascr#8 response**. **(A)** Raw dwell times and **(B)** Log(fold-change) of *dmsr-12* knockout
633 and transgenic rescue (WorEx54) animals. **(C)** Expression of WorEx54 (p*dmsr-12*::*dmsr-*
634 *12*::GFP) in CEM DL and CEM DR. Anterior/Posterior and Dorsal/Ventral axes denoted. **(D)** Raw
635 dwell times and **(F)** Log(fold-change) of *him-5* and *dmsr-12;srw-97* animals in response to the
636 structurally related attracted pheromone, ascr#3. **(E)** Structural comparison of ascr#8 (top) and
637 ascr#3 (bottom). Error bars denote SEM. $n \geq 5$. **(A, D)** ANOVA followed by Dunnett's post-hoc
638 test or Friedman test followed by Dunn's post-hoc test (within strain), **(B)** ANOVA, followed by
639 Bonferroni post-hoc test (between strain log(fold-change) values), **(F)** Student's t-test between
640 strain log(fold-change) values. * $p < 0.05$.
641
642 **Figure 6. Phylogenetic analysis of ascr#8-receptor candidate paralogs across the**
643 ***Caenorhabditis* genus.** **(A)** The phylogeny of *Cel_srw-97* reveals a *C. inopinata*-specific
644 amplification of *Cel_srw-98*. **(B)** The phylogeny of *Cel_dmsr-12* shows conserved counts of
645 orthologs across the genus. Genes for *C. elegans* denoted in purple; *C. inopinata* in pink, *C. nigoni*
646 in light blue, *C. briggsae* in dark blue, *C. japonica* in red, and *C. tropicalis* in dark green. Distance
647 reference bars (0.1) depict substitutions per site.

648 **REFERENCES**

649 Apirson, E. Z., and I. Ruvinsky, 2019a Coordinated behavioral and physiological responses to a
650 social signal are regulated by a shared neuronal circuit. Curr Biol.
651 Apirson, E. Z., and I. Ruvinsky, 2019b Dynamic regulation of adult-specific functions of the
652 nervous system by signaling from the reproductive system. Curr Biol.
653 Aprison, E. Z., and I. Ruvinsky, 2015 Sex Pheromones of *C. elegans* Males Prime the Female
654 Reproductive System and Ameliorate the Effects of Heat Stress. PLoS Genet 11**:**
655 e1005729.
656 Aprison, E. Z., and I. Ruvinsky, 2017 Counteracting Ascarosides Act through Distinct Neurons to
657 Determine the Sexual Identity of *C. elegans* Pheromones. Curr Biol 27**:** 2589-2599.e2583.
658 Artyukhin, A. B., Y. K. Zhang, A. E. Akagi, O. Panda, P. W. Sternberg *et al.*, 2018 Metabolomic
659 "Dark Matter" Dependent on Peroxisomal beta-Oxidation in *Caenorhabditis elegans*. J Am
660 Chem Soc 140**:** 2841-2852.
661 Bae, Y. K., H. Qin, K. M. Knobel, J. Hu, J. L. Rosenbaum *et al.*, 2006 General and cell-type
662 specific mechanisms target TRPP2/PKD-2 to cilia. Development 133**:** 3859-3870.
663 Boulin, T., J. F. Etchberger and O. Hobert, 2006 Reporter gene fusions. WormBook**:** 1-23.
664 Butcher, R. A., 2017 Small-molecule pheromones and hormones controlling nematode
665 development. Nat Chem Biol 13**:** 577-586.
666 Butcher, R. A., M. Fujita, F. C. Schroeder and J. Clardy, 2007 Small-molecule pheromones that
667 control dauer development in *Caenorhabditis elegans*. Nat Chem Biol 3**:** 420-422.
668 Butcher, R. A., J. R. Ragains and J. Clardy, 2009 An indole-containing dauer pheromone
669 component with unusual dauer inhibitory activity at higher concentrations. Org Lett 11**:**
670 3100-3103.

671 Butcher, R. A., J. R. Ragains, E. Kim and J. Clardy, 2008 A potent dauer pheromone component
672 in Caenorhabditis elegans that acts synergistically with other components. Proc Natl Acad
673 Sci U S A 105**:** 14288-14292.
674 Capella-Gutiérrez, S., J. M. Silla-Martínez and T. Gabaldón, 2009 trimAl: a tool for automated
675 alignment trimming in large-scale phylogenetic analyses. Bioinformatics (Oxford,
676 England) 25**:** 1972-1973.
677 Choe, A., S. H. von Reuss, D. Kogan, R. B. Gasser, E. G. Platzer *et al.*, 2012 Ascaroside Signaling
678 is Widely Conserved Among Nematodes. Current Biology 22**:** 772-780.
679 Chute, C. D., E. M. DiLoreto, Y. K. Zhang, D. K. Reilly, D. Rayes *et al.*, 2019 Co-option of
680 neurotransmitter signaling for inter-organismal communication in *C. elegans*. Nat
681 Commun 10**:** 3186.
682 Cochella, L., B. Tursun, Y. W. Hsieh, S. Galindo, R. J. Johnston *et al.*, 2014 Two distinct types of
683 neuronal asymmetries are controlled by the *Caenorhabditis elegans* zinc finger
684 transcription factor die-1. Genes Dev 28**:** 34-43.
685 Dong, C., F. Dolke and S. H. von Reuss, 2016 Selective MS screening reveals a sex pheromone in
686 Caenorhabditis briggsae and species-specificity in indole ascaroside signalling. Org
687 Biomol Chem 14**:** 7217-7225.
688 Dong, C., D. K. Reilly, C. Bergame, F. Dolke, J. Srinivasan *et al.*, 2018 Comparative Ascaroside
689 Profiling of *Caenorhabditis* Exometabolomes Reveals Species-Specific (ω) and (ω - 2)-
690 Hydroxylation Downstream of Peroxisomal beta-Oxidation. J Org Chem.
691 Eddy, S. R., 2009 A new generation of homology search tools based on probabilistic inference.
692 Genome informatics. International Conference on Genome Informatics 23**:** 205-211.

693 Emms, D. M., and S. Kelly, 2015 OrthoFinder: solving fundamental biases in whole genome
694 comparisons dramatically improves orthogroup inference accuracy. Genome Biology 16**:**
695 157.
696 Emms, D. M., and S. Kelly, 2019 OrthoFinder: phylogenetic orthology inference for comparative
697 genomics. Genome Biology 20**:** 238.
698 Fagan, K. A., J. Luo, R. C. Lagoy, F. C. Schroeder, D. R. Albrecht *et al.*, 2018 A Single-Neuron
699 Chemosensory Switch Determines the Valence of a Sexually Dimorphic Sensory Behavior.
700 Curr Biol 28**:** 902-914.e905.
701 Finn, R. D., P. Coggill, R. Y. Eberhardt, S. R. Eddy, J. Mistry *et al.*, 2016 The Pfam protein
702 families database: towards a more sustainable future. Nucleic acids research 44**:** D279-
703 D285.
704 Fraser, A. G., R. S. Kamath, P. Zipperlen, M. Martinez-Campos, M. Sohrmann *et al.*, 2000
705 Functional genomic analysis of *C. elegans* chromosome I by systematic RNA interference.
706 Nature 408**:** 325-330.
707 Fuxman Bass, J. I., A. M. Tamburino, A. Mori, N. Beittel, M. T. Weirauch *et al.*, 2014
708 Transcription factor binding to Caenorhabditis elegans first introns reveals lack of
709 redundancy with gene promoters. Nucleic Acids Res 42**:** 153-162.
710 Gene Ontology, C., 2021 The Gene Ontology resource: enriching a GOld mine. Nucleic acids
711 research 49**:** D325-D334.
712 Goodman, M. B., D. H. Hall, L. Avery and S. R. Lockery, 1998 Active currents regulate sensitivity
713 and dynamic range in *C. elegans* neurons. Neuron 20**:** 763-772.

714 Gordon, K. L., R. K. Arthur and I. Ruvinsky, 2015 Phylum-Level Conservation of Regulatory
715 Information in Nematodes despite Extensive Non-coding Sequence Divergence. PLoS
716 genetics 11**:** e1005268-e1005268.
717 Greene, J. S., M. Brown, M. Dobosiewicz, I. G. Ishida, E. Z. Macosko *et al.*, 2016b Balancing
718 selection shapes density-dependent foraging behaviour. Nature 539**:** 254-258.
719 Greene, J. S., M. Dobosiewicz, R. A. Butcher, P. T. McGrath and C. I. Bargmann, 2016a
720 Regulatory changes in two chemoreceptor genes contribute to a *Caenorhabditis elegans*
721 QTL for foraging behavior. Elife 5.
722 Harris, T. W., V. Arnaboldi, S. Cain, J. Chan, W. J. Chen *et al.*, 2020 WormBase: a modern Model
723 Organism Information Resource. Nucleic Acids Res 48**:** D762-d767.
724 Hobert, O., 2013 The neuronal genome of *Caenorhabditis elegans*. WormBook**:** 1-106.
725 Houck, L., C. Palmer, R. Watts, S. Arnold, P. Feldhoff *et al.*, 2007 A new vertebrate courtship
726 pheromone, PMF, affects female receptivity in a terrestrial salamander. Animal Behaviour
727 73**:** 315-320.
728 Howe, K. L., B. J. Bolt, S. Cain, J. Chan, W. J. Chen *et al.*, 2016 WormBase 2016: expanding to
729 enable helminth genomic research. Nucleic acids research 44**:** D774-D780.
730 Hrus, A., G. Lau, H. Hutter, S. Schenk, J. Ferralli *et al.*, 2007 *C. elegans* Agrin Is Expressed in
731 Pharynx, IL1 Neurons and Distal Tip Cells and Does Not Genetically Interact with Genes
732 Involved in Synaptogenesis or Muscle Function. PLOS ONE 2**:** e731.
733 Jang, Y. H., H. S. Chae and Y. J. Kim, 2017 Female-specific myoinhibitory peptide neurons
734 regulate mating receptivity in *Drosophila melanogaster*. Nat Commun 8**:** 1630.

735 Jee, C., J. Lee, J. P. Lim, D. Parry, R. O. Messing *et al.*, 2013 SEB-3, a CRF receptor-like GPCR,
736 regulates locomotor activity states, stress responses, and ethanol tolerance in *C. elegans*.
737 Genes, brain, and behavior 12**:** 10.1111/j.1601-1183X.2012.00829.x.
738 Kaletsky, R., V. Lakhina, R. Arey, A. Williams, J. Landis *et al.*, 2016 The C. elegans adult
739 neuronal IIS/FOXO transcriptome reveals adult phenotype regulators. Nature 529**:** 92-96.
740 Käll, L., A. Krogh and E. L. L. Sonnhammer, 2004 A combined transmembrane topology and
741 signal peptide prediction method. Journal of molecular biology 338**:** 1027-1036.
742 Kalyaanamoorthy, S., B. Q. Minh, T. K. F. Wong, A. von Haeseler and L. S. Jermiin, 2017
743 ModelFinder: fast model selection for accurate phylogenetic estimates. Nature methods
744 14**:** 587-589.
745 Kamath, R. S., A. G. Fraser, Y. Dong, G. Poulin, R. Durbin *et al.*, 2003 Systematic functional
746 analysis of the *Caenorhabditis elegans* genome using RNAi. Nature 421**:** 231-237.
747 Katoh, K., and D. M. Standley, 2013 MAFFT multiple sequence alignment software version 7:
748 improvements in performance and usability. Molecular biology and evolution 30**:** 772-780.
749 Kim, K., K. Sato, M. Shibuya, D. M. Zeiger, R. A. Butcher *et al.*, 2009 Two Chemoreceptors
750 Mediate Developmental Effects of Dauer Pheromone in *C. elegans*. Science 326**:** 994-998.
751 Krishnan, A., M. S. Almén, R. Fredriksson and H. B. Schiöth, 2014 Insights into the Origin of
752 Nematode Chemosensory GPCRs: Putative Orthologs of the Srw Family Are Found across
753 Several Phyla of Protostomes. PLoS ONE 9**:** e93048.
754 Langmead, B., and S. L. Salzberg, 2012 Fast gapped-read alignment with Bowtie 2. Nature
755 methods 9**:** 357-359.

Lee, H., M.-k. Choi, D. Lee, H.-s. Kim, H. Hwang *et al.*, 2012 Nictation, a dispersal behavior of the nematode Caenorhabditis elegans, is regulated by IL2 neurons. Nature Neuroscience 15**:** 107-112.

Lemoine, F., J. B. Domelevo Entfellner, E. Wilkinson, D. Correia, M. Dávila Felipe *et al.*, 2018 Renewing Felsenstein's phylogenetic bootstrap in the era of big data. Nature 556**:** 452-456.

Li, B., and C. N. Dewey, 2011 RSEM: accurate transcript quantification from RNA-Seq data with or without a reference genome. BMC bioinformatics 12**:** 323-323.

Li, H., B. Handsaker, A. Wysoker, T. Fennell, J. Ruan *et al.*, 2009 The Sequence Alignment/Map format and SAMtools. Bioinformatics (Oxford, England) 25**:** 2078-2079.

Ludewig, A. H., A. B. Artyukhin, E. Z. Aprison, P. R. Rodrigues, D. C. Pulido *et al.*, 2019 An excreted small molecule promotes *C. elegans* reproductive development and aging. Nat Chem Biol 15**:** 838-845.

Lupas, A., 1996 Prediction and analysis of coiled-coil structures. Methods in enzymology 266**:** 513-525.

Madeira, F., Y. M. Park, J. Lee, N. Buso, T. Gur *et al.*, 2019 The EMBL-EBI search and sequence analysis tools APIs in 2019. Nucleic acids research 47**:** W636-W641.

McGrath, P. T., and I. Ruvinsky, 2019 A primer on pheromone signaling in *Caenorhabditis elegans* for systems biologists. Curr Opin Syst Biol 13**:** 23-30.

McGrath, P. T., Y. Xu, M. Ailion, J. L. Garrison, R. A. Butcher *et al.*, 2011 Parallel evolution of domesticated *Caenorhabditis* species targets pheromone receptor genes. Nature 477**:** 321-325.

Narayan, A., G. Laurent and P. W. Sternberg, 2011 Transfer characteristics of a thermosensory synapse in *Caenorhabditis elegans*. Proceedings of the National Academy of Sciences of the United States of America 108**:** 9667-9672.

Narayan, A., V. Venkatachalam, O. Durak, D. K. Reilly, N. Bose *et al.*, 2016 Contrasting responses within a single neuron class enable sex-specific attraction in *Caenorhabditis elegans*. Proc Natl Acad Sci U S A 113**:** E1392-1401.

Nguyen, L.-T., H. A. Schmidt, A. von Haeseler and B. Q. Minh, 2015 IQ-TREE: a fast and effective stochastic algorithm for estimating maximum-likelihood phylogenies. Molecular biology and evolution 32**:** 268-274.

Noble, L. M., J. Yuen, L. Stevens, N. Moya, R. Persaud *et al.*, 2021 Selfing is the safest sex for Caenorhabditis tropicalis. Elife 10.

Park, D., I. O'Doherty, R. K. Somvanshi, A. Bethke, F. C. Schroeder *et al.*, 2012 Interaction of structure-specific and promiscuous G-protein-coupled receptors mediates small-molecule signaling in *Caenorhabditis elegans*. PNAS 109**:** 9917-9922.

Peden, E. M., and M. M. Barr, 2005 The KLP-6 kinesin is required for male mating behaviors and polycystin localization in *Caenorhabditis elegans*. Curr Biol 15.

Poole, R. J., E. Bashllari, L. Cochella, E. B. Flowers and O. Hobert, 2011 A Genome-Wide RNAi Screen for Factors Involved in Neuronal Specification in *Caenorhabditis elegans*. PLoS Genet 7**:** e1002109.

Powell, S., D. Szklarczyk, K. Trachana, A. Roth, M. Kuhn *et al.*, 2012 eggNOG v3.0: orthologous groups covering 1133 organisms at 41 different taxonomic ranges. Nucleic acids research 40**:** D284-D289.

799 Pungaliya, C., J. Srinivasan, B. W. Fox, R. U. Malik, A. H. Ludewig *et al.*, 2009 A shortcut to
800 identifying small molecule signals that regulate behavior and development in
801 *Caenorhabditis elegans*. Proceedings of the National Academy of Sciences of the United
802 States of America 106**:** 7708-7713.
803 Ragsdale, E. J., M. R. Muller, C. Rodelsperger and R. J. Sommer, 2013 A developmental switch
804 coupled to the evolution of plasticity acts through a sulfatase. Cell 155**:** 922-933.
805 Reilly, D. K., D. E. Lawler, D. R. Albrecht and J. Srinivasan, 2017 Using an Adapted Microfluidic
806 Olfactory Chip for the Imaging of Neuronal Activity in Response to Pheromones in Male
807 *C. Elegans* Head Neurons. Journal of Visualized Experiments**:** e56026.
808 Reilly, D. K., E. J. McGlame, E. Vandewyer, A. N. Robidoux, C. S. Muirhead *et al.*, 2021 Distinct
809 neuropeptide-receptor modules regulate a sex-specific behavioral response to a
810 pheromone. Communications Biology 4**:** 1018.
811 Reilly, D. K., L. J. Randle and J. Srinivasan, 2019 Evolution of hermaphroditism decreases
812 efficacy of Ascaroside#8-mediated mate attraction in *Caenorhabditis* nematodes.
813 microPublication Biology.
814 Robertson, H. M., and J. H. Thomas, 2006 The putative chemoreceptor families of *C. elegans*.
815 WormBook**:** 1-12.
816 Rual, J. F., J. Ceron, J. Koreth, T. Hao, A. S. Nicot *et al.*, 2004 Toward improving *Caenorhabditis*
817 *elegans* phenome mapping with an ORFeome-based RNAi library. Genome Res 14**:** 2162-
818 2168.
819 Sammut, M., S. J. Cook, K. C. Q. Nguyen, T. Felton, D. H. Hall *et al.*, 2015 Glia-derived neurons
820 are required for sex-specific learning in C. elegans. Nature 526**:** 385-390.

821 Schmitz, C., P. Kinge and H. Hutter, 2007 Axon guidance genes identified in a large-scale RNAi
822 screen using the RNAi-hypersensitive *Caenorhabditis elegans* strain *nre-1(hd20) lin-*
823 *15b(hd126)*. Proceedings of the National Academy of Sciences 104**:** 834-839.
824 Schroeder, N. E., R. J. Androwski, A. Rashid, H. Lee, J. Lee *et al.*, 2013 Dauer-specific dendrite
825 arborization in C. elegans is regulated by KPC-1/Furin. Curr Biol 23**:** 1527-1535.
826 Schwarz, E. M., M. Kato and P. W. Sternberg, 2012 Functional transcriptomics of a migrating cell
827 in Caenorhabditis elegans. Proceedings of the National Academy of Sciences of the United
828 States of America 109**:** 16246-16251.
829 Taylor, S. R., G. Santpere, A. Weinreb, A. Barrett, M. B. Reilly *et al.*, 2021 Molecular topography
830 of an entire nervous system. Cell 184**:** 4329-4347.e4323.
831 Tenor, J. L., and A. Aballay, 2008 A conserved Toll-like receptor is required for Caenorhabditis
832 elegans innate immunity. EMBO Rep 9**:** 103-109.
833 von Reuss, S. H., N. Bose, J. Srinivasan, J. J. Yim, J. C. Judkins *et al.*, 2012 Comparative
834 Metabolomics Reveals Biogenesis of Ascarosides, a Modular Library of Small-Molecule
835 Signals in *C. elegans*. Journal of the American Chemical Society 134**:** 1817-1824.
836 von Reuss, S. H., and F. C. Schroeder, 2015 Combinatorial chemistry in nematodes: modular
837 assembly of primary metabolism-derived building blocks. Natural product reports 32**:** 994-
838 1006.
839 Wang, J., R. Kaletsky, M. Silva, A. Williams, L. A. Haas *et al.*, 2015 Cell-Specific Transcriptional
840 Profiling of Ciliated Sensory Neurons Reveals Regulators of Behavior and Extracellular
841 Vesicle Biogenesis. Curr Biol 25**:** 3232-3238.

842 Wang, J., M. Silva, L. A. Haas, N. S. Morsci, K. C. Q. Nguyen *et al.*, 2014 *C. elegans* Ciliated
843 Sensory Neurons Release Extracellular Vesicles that Function in Animal Communication.
844 Current Biology 24**:** 518-525.
845 Wang, X., J. F. Greenberg and H. M. Chamberlin, 2004 Evolution of regulatory elements
846 producing a conserved gene expression pattern in *Caenorhabditis*. Evolution &
847 Development 6**:** 237-245.
848 White, J. G., E. Southgate, J. N. Thomas and S. Brenner, 1986 The structure of the nervous system
849 of the nematode Caernorhabditis elegans. Phil Trans Royal Soc Lon 314B.
850 Wootton, J. C., 1994 Non-globular domains in protein sequences: automated segmentation using
851 complexity measures. Computers & chemistry 18**:** 269-285.
852 Zhang, Y. K., D. K. Reilly, J. Yu, J. Srinivasan and F. C. Schroeder, 2019 Photoaffinity probes for
853 nematode pheromone receptor identification. Journal of Organic & Biomolecular
854 Chemistry**:** 10.1039/C1039OB02099C.
855 Zhang, Y. K., M. A. Sanchez-Ayala, P. W. Sternberg, J. Srinivasan and F. C. Schroeder, 2017
856 Improved Synthesis for Modular Ascarosides Uncovers Biological Activity. Org Lett 19**:**
857 2837-2840.
858 Zwaal, R. R., J. E. Mendel, P. W. Sternberg and R. H. Plasterk, 1997 Two neuronal G proteins are
859 involved in chemosensation of the *Caenorhabditis* elegans Dauer-inducing pheromone.
860 Genetics 145**:** 715-727.

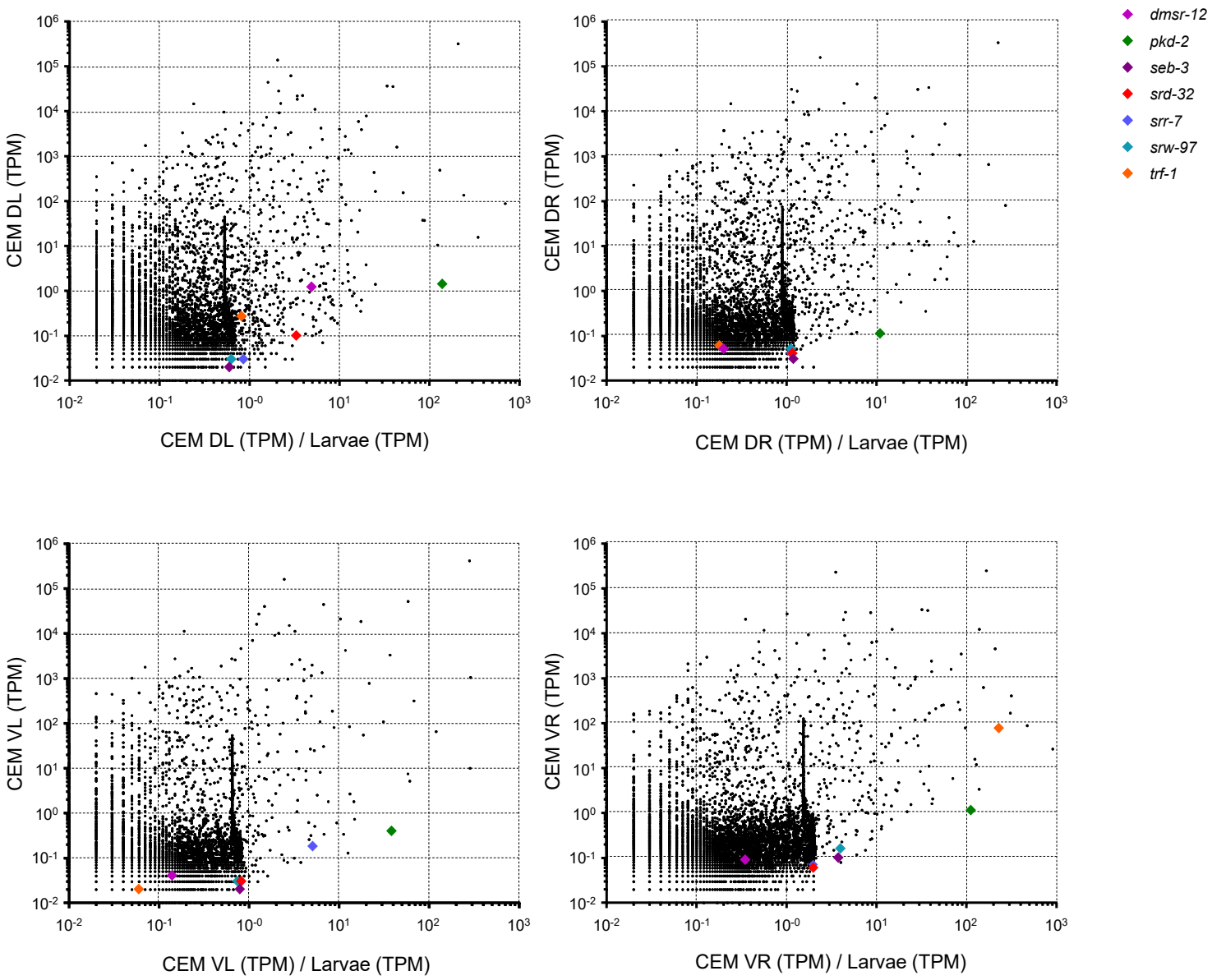
dmsr-12
pkd-2
seb-3
srd-32
srr-7
srw-97
trf-1
CEM DL (TPM)
CEM DL (TPM) / Larvae (TPM)
CEM DR (TPM)
CEM DR (TPM) / Larvae (TPM)
CEM VL (TPM)
CEM VL (TPM) / Larvae (TPM)
CEM VR (TPM)
CEM VR (TPM) / Larvae (TPM)

Figure - 1

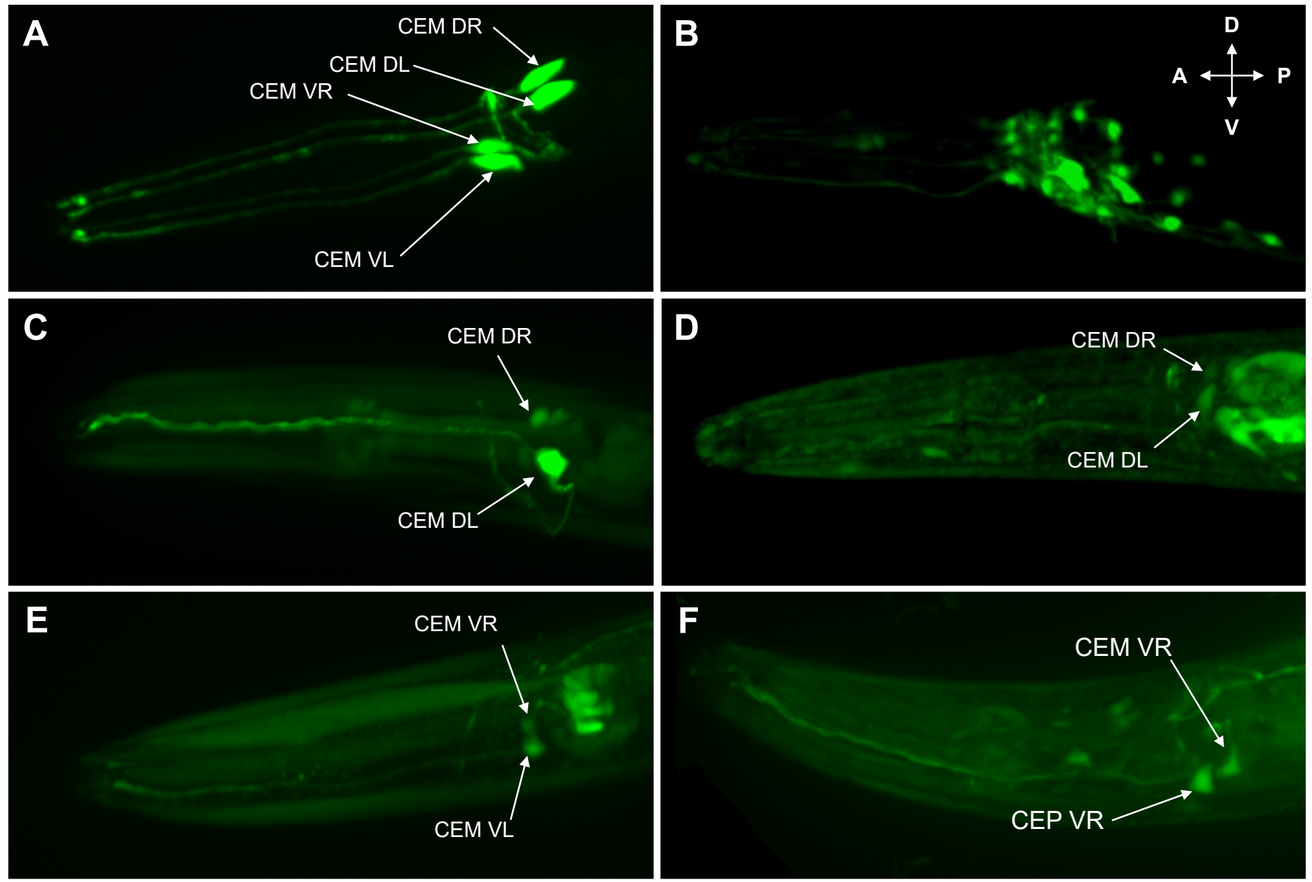
A
CEM DR
CEM DL
CEM VR
CEM VL
B
D
A
P
V
C
CEM DR
CEM DL
D
CEM DR
CEM DL
E
CEM VR
CEM VL
F
CEM VR
CEP VR

Figure - 2

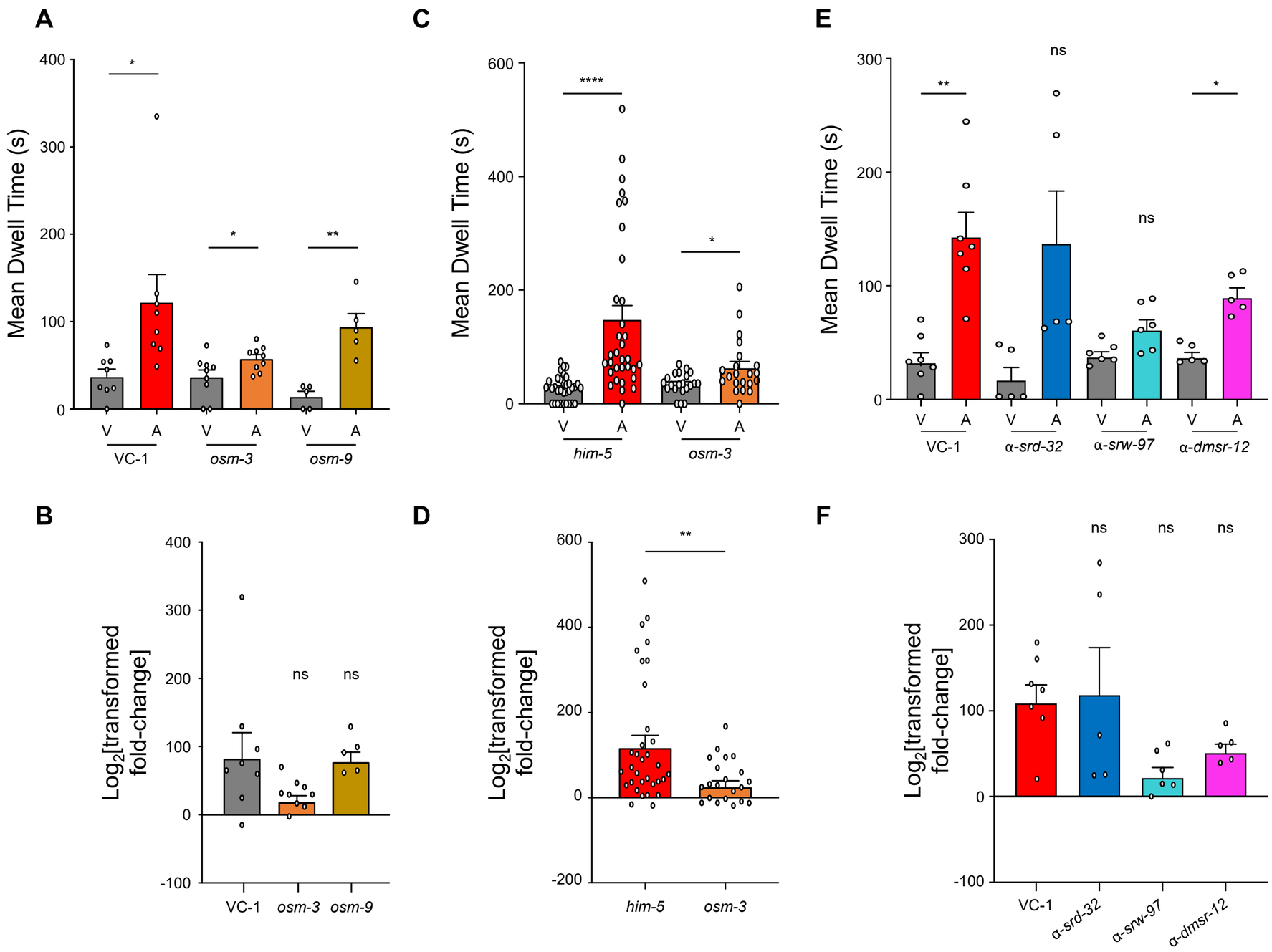
A
Mean Dwell Time (s)
400
300
200
100
0
*
*
**
V
A
V
A
V
A
VC-1
osm-3
osm-9
B
Log2[transformed fold-change]
400
300
200
100
0
-100
ns
ns
VC-1
osm-3
osm-9
C
Mean Dwell Time (s)
600
400
200
0
****
*
V
A
V
A
him-5
osm-3
D
Log2[transformed fold-change]
600
400
200
0
-200
**
him-5
osm-3
E
Mean Dwell Time (s)
300
200
100
0
ns
ns
**
*
V
A
V
A
V
A
V
A
VC-1
α-srd-32
α-srw-97
α-dmsr-12
F
Log2[transformed fold-change]
300
200
100
0
-100
ns
ns
ns
VC-1
α-srd-32
α-srw-97
α-dmsr-12

Figure - 3

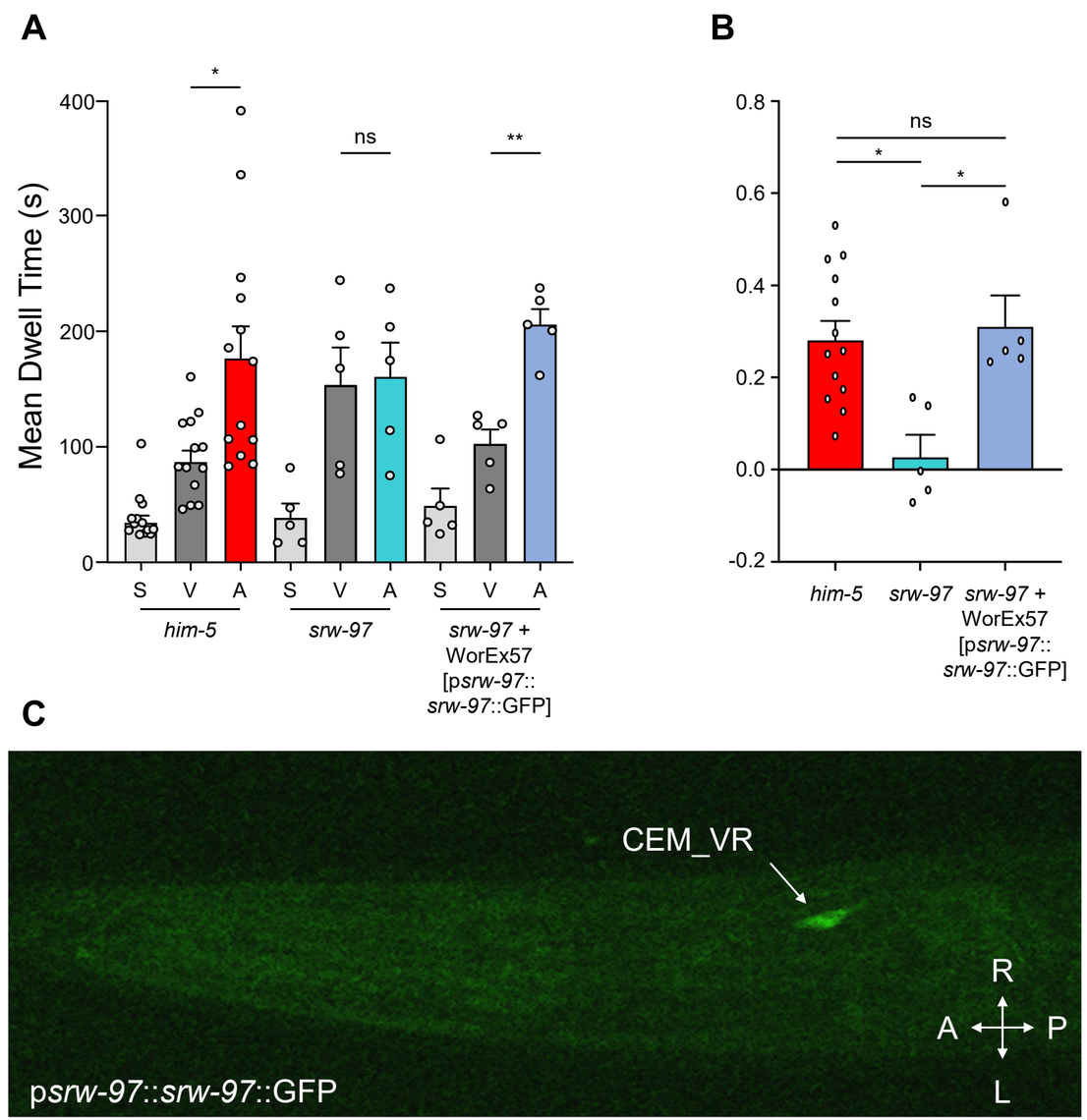
A
Mean Dwell Time (s)
400
300
200
100
0
*
ns
**
S V A
him-5
S V A
srw-97
S V A
srw-97 +
WorEx57
[psrw-97::
srw-97::GFP]
B
0.8
0.6
0.4
0.2
0.0
-0.2
ns
*
*
him-5
srw-97
srw-97 +
WorEx57
[psrw-97::
srw-97::GFP]
C
CEM_VR
R
A
P
L
psrw-97::srw-97::GFP

Figure - 4

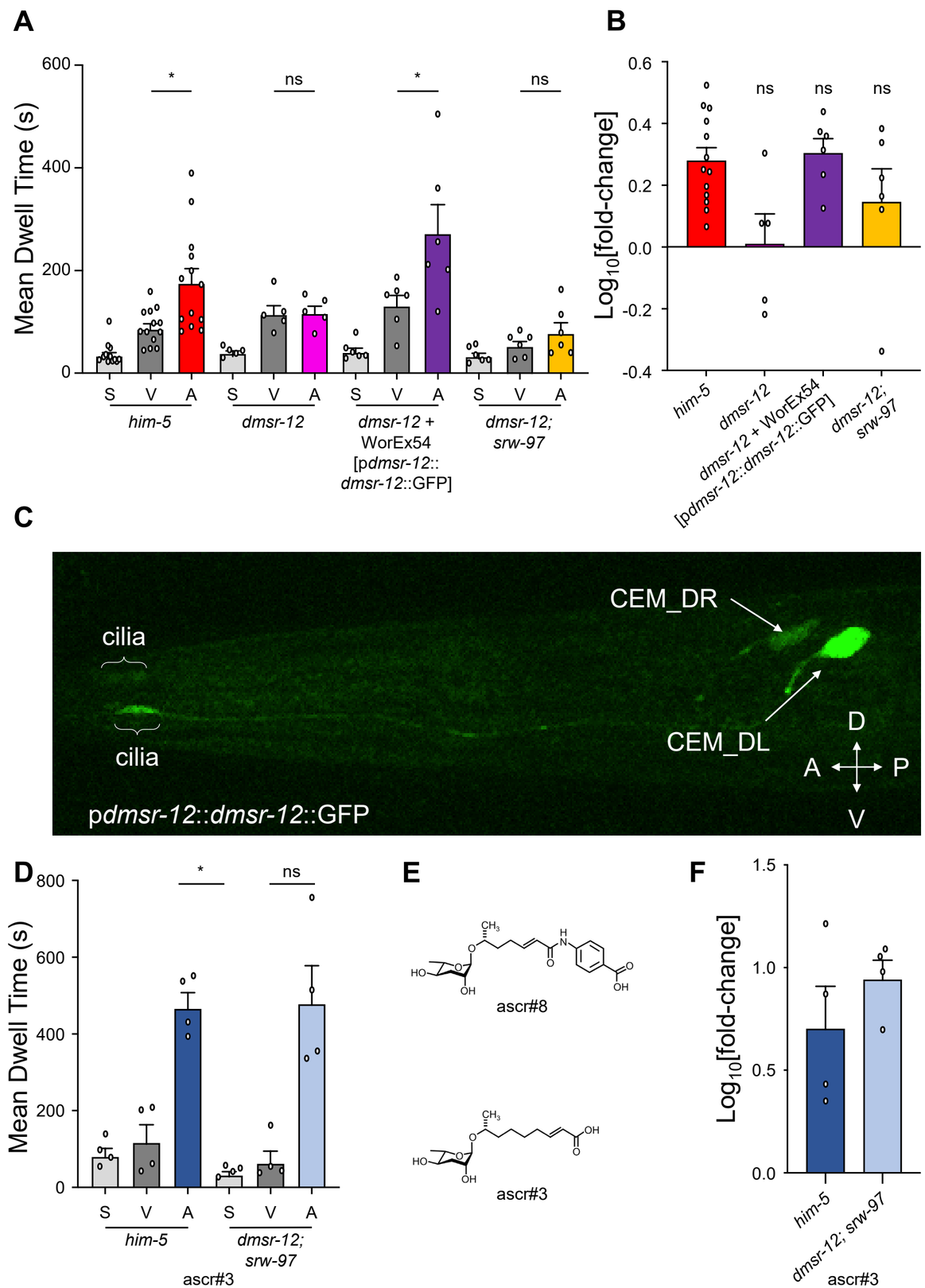
A
Mean Dwell Time (s)
600
400
200
0
*
ns
*
ns
S V A S V A S V A S V A
him-5
dmsr-12
dmsr-12 + WorEx54 [pdmsr-12::dmsr-12::GFP]
dmsr-12; srw-97
B
Log10[fold-change]
0.6
0.4
0.2
0.0
-0.2
-0.4
ns
ns
ns
him-5
dmsr-12
dmsr-12 + WorEx54 [pdmsr-12::dmsr-12::GFP]
dmsr-12; srw-97
C
CEM_DR
cilia
cilia
CEM_DL
D
A
P
V
pdmsr-12::dmsr-12::GFP
D
Mean Dwell Time (s)
800
600
400
200
0
*
ns
S V A S V A
him-5
dmsr-12; srw-97
ascr#3
E
ascr#8
ascr#3
F
Log10[fold-change]
1.5
1.0
0.5
0.0
him-5
dmsr-12; srw-97
ascr#3

Figure - 5

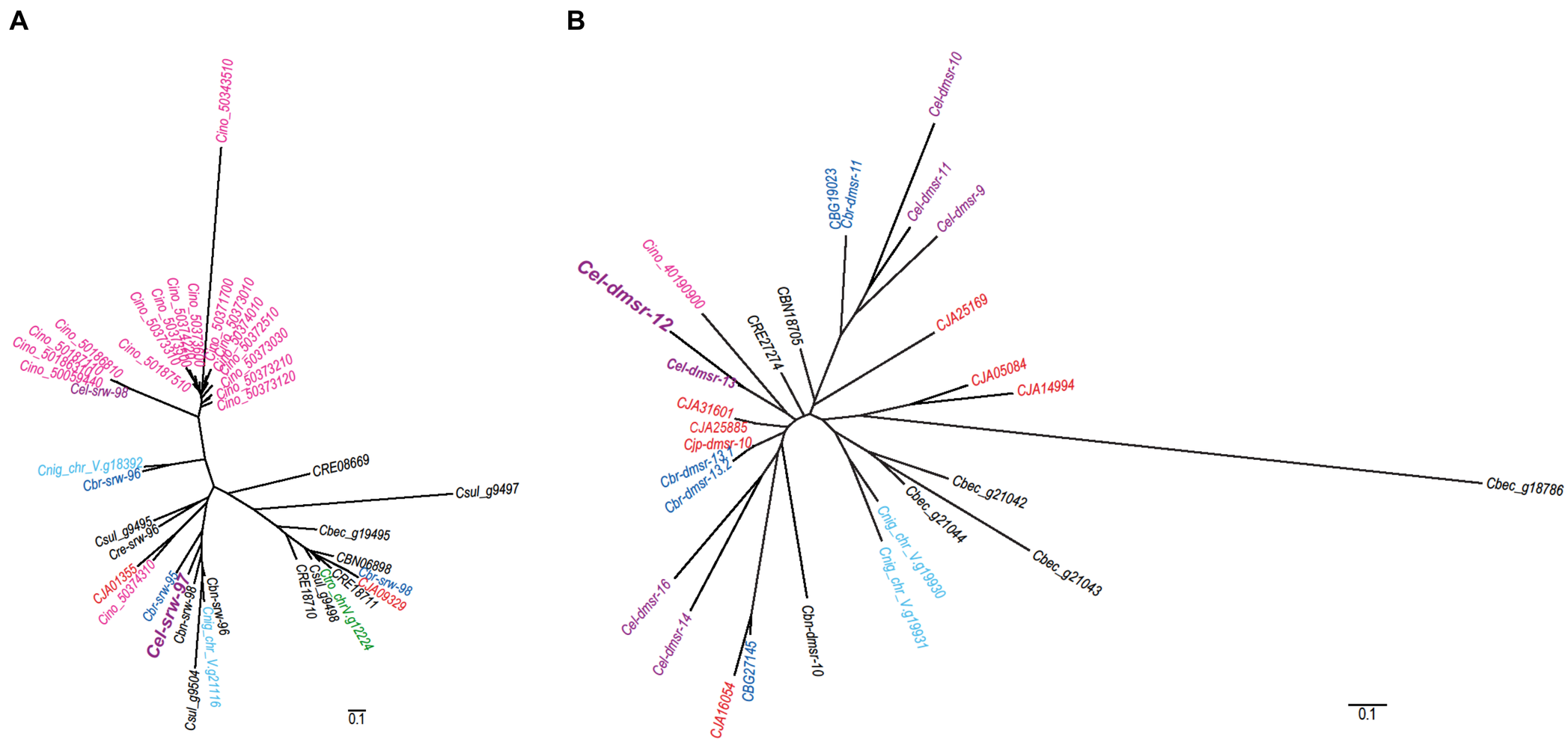
A
Cino_50343510
Cino_50371700
Cino_50373010
Cino_50374010
Cino_50372510
Cino_50373030
Cino_50373210
Cino_50373120
Cino_50187510
Cino_50186810
Cino_50187110
Cino_50186410
Cino_50059440
Cel-srw-98
Cnig_chr_V.g18392
Cbr-srw-96
CRE08669
Csul_g9497
Csul_g9495
Cre-srw-96
Cbec_g19495
CBN06898
Cbr-srw-98
CJA09329
CRE18711
Cino_chrV.g1224
Csul_g9498
CRE18710
CJA01355
Cino_50374310
Cbr-srw-95
Cel-srw-97
Cbr-srw-98
Cbr-srw-96
Cnig_chr_V.g21116
Csul_g9504
0.1
B
Cel-dmsr-10
CBG19023
Cbr-dmsr-11
Cel-dmsr-11
Cel-dmsr-9
Cino_40190900
Cel-dmsr-12
CBN18705
CRE27274
CJA25169
Cel-dmsr-13
CJA05084
CJA14994
CJA31601
CJA25885
Cjp-dmsr-10
Cbr-dmsr-13
Cbr-dmsr-13.2
Cbec_g21042
Cbec_g18786
Cbec_g21044
Cbec_g21043
Cnig_chr_V.g19930
Cnig_chr_V.g19931
Cel-dmsr-16
Cel-dmsr-14
Cbr-dmsr-10
CBG27145
CJA16054
0.1

Figure - 6